

Contents lists available at ScienceDirect

Journal of Environmental Chemical Engineering

journal homepage: www.elsevier.com/locate/jece





Degradation of dissolved RDX, NQ, and DNAN by cathodic processes in an electrochemical flow-through reactor

Nazli Rafei Dehkordi, Michael Knapp, Patrick Compton, Loretta A. Fernandez, Akram N. Alshawabkeh, Philip Larese-Casanova *

Department of Civil and Environmental Engineering, Northeastern University, Boston, MA, USA

ARTICLE INFO

Editor: Dr. G. Palmisano

Keywords: Explosives Electrochemical reduction Cathodic processes Alkaline hydrolysis RDX

ABSTRACT

Both legacy munitions compounds (e.g., RDX) and new insensitive high explosives (e.g. DNAN, NQ) are being manufactured and utilized concurrently, and there exists a need for wastewater treatment systems that are able to degrade both classes of explosives. Electrochemical systems offer treatment possibilities using inexpensive materials and no chemical additions. Electrochemically induced removal of RDX, NQ, and DNAN were separately studied within an electrochemical plug flow reactor hosting a stainless steel (SS) cathode and downstream Ti/ MMO anode. Varying wire mesh cathodes and operating conditions were evaluated in an effort to identify the optimal cathode material, to determine the relative contributions of cathodically-induced removal processes, to shorten time to steady-state removal conditions, and to find practical ranges of operating conditions. Applied current allowed the cathode to support munitions removal mainly by direct reduction at the cathode surface, and the secondary reactions of cathodically-induced alkaline hydrolysis and catalytic hydrogenation by adsorbed H on Ni-containing cathode surfaces might contribute to some munitions degradation. The optimal cathode material was identified as SS grade 316, possibly due to its superior Ni content and lack of corrosion protection coating. Higher current, longer cathode length, and smaller mesh pore sizes resulted in slightly greater removal extents and shorter acclimation times to steady state removal conditions, but there are practical upper limits to these properties. Higher Ni content within SS improved RDX and NO removal but does not affect DNAN removal. Prolonged use of SS grade 316 showed no debilitating changes in electrical performance or chemical content.

1. Introduction

The manufacturing and application of explosives can result in contaminated water and soil, posing risks to human health and to aquatic and terrestrial life [1–5]. In particular, manufacturing wastewaters may contain high concentrations of explosive compounds near solubility limits. Wastes from assembling formulations may also contain mixtures of explosives compounds. Formulations can be composed of both legacy munitions constituents such as RDX (hexahydro-1,3,5-trinitro-1,3,5-triazine) and new insensitive high explosives (IHEs) such as DNAN (2,4-dinitroanisole) or NQ (nitroguanidine). RDX, DNAN, and NQ are all C-N compounds containing nitro groups, but their physicochemical properties like solubility can vary widely when present in wastewaters [6].

Therefore, treatment methods are needed that can be applicable to explosive compounds with diverse properties and potentially diverse reactivities. Conventional treatment methods have been proven for legacy munitions, but they may still need adaptation to IHEs or could have some limitations. Physical removal is possible by activated carbon [7], but requires further treatment of spent media. Chemical treatment such as reduction by zero-valent iron [8–10] or alkaline hydrolysis [11–13] requires chemical addition and possible removal of Fe corrosion products. Advanced oxidation processes, although fast [14–16] are energy-intensive. Biological processes are not proven yet for many new IHEs.

Electrochemical treatment systems represent an alternative process that could offer some advantages for explosives wastewater treatment. Hosting reduction or oxidation reactions at electrodes could avoid chemical additions and reagent by-products, transformation could potentially be achieved entirely in situ, and current requirements may be low-energy. Electrochemical transformation of the explosives RDX [15,17–22] TNT [18,19,23,24], 2,4-DNT [18,19,24,25], 2,6-DNT [25]

^{*} Correspondence to: Department of Civil & Environmental Engineering, Northeastern University, 400 Snell Engineering, Boston, MA 02115, USA. E-mail address: p.laresecasanova@northestern.edu (P. Larese-Casanova).

and NTO [26] have been reported, but studies of DNAN and NQ are lacking. Cathodic reduction of RDX tends to occur by reducing nitro groups to nitroso or amine groups and is a common initiation point of degradation [17,19,27]. Anodic oxidation of the explosive or its intermediates is also possible [19,27,28]. It has been recognized that first reducing explosives makes intermediate compounds that are more susceptible to oxidation reactions, and the combined strategy of reduction followed by oxidation in electrochemical systems [10,18,26,29,30]. Other systems using this strategy [10,27,29,31,32] have been found to more completely mineralize explosives.

This study examines the reductive treatment of these explosives occurring by cathodic processes within a flow-through column electrochemical reactor. Flowing water through a separated cathode and anode allows for localized regions of reduction at the cathode and oxidation at the anode. When operating potentials exceed that for water electrolysis, H⁺ reduction to H₂ gas creates alkaline conditions which could potentially promote alkaline hydrolysis of explosives as a second reaction pathway. Electrolytic generation of alkaline conditions has previously been noted to contribute to RDX degradation within sand columns with redox conditions manipulated electrochemically [20]. How alkaline the electrochemical conditions become, and much the alkaline hydrolysis process contributes to explosives degradation within the cathode region, are therefore important questions. One drawback of flow-through column reactors, though, is that although the current can be applied instantly, the time to steady-state cathodic processes can be significantly long, up to several hours [33,34]. In addition, longer cathodes allow for more contact time in the cathode, and so less expensive cathode materials are desired. So far for explosives, the more expensive Ti/MMO electrodes [15,19-21] zero-valent metals [25], and carbon-based materials [17,18,24,26,28] have been used.

More recently, stainless steel (SS) has been evaluated as a costeffective alternative electrode material for cathodic reduction of trichloroethylene (TCE) [33] and RDX [17,27]. SS is a widely available material in various compositions, mesh sizes, and weaves. SS is an Fe-C metal allow with varying metal impurities for strength or corrosion resistance purposes. When Ni is present, it can act as a noble metal that can adsorb H2 to form atomic hydrogen (Hads) and promote catalytic hydrogenation as a secondary reductive process. Hads on nickel has previously been shown to reduce RDX [35], and some TCE reduction on SS cathodes has been attributed to Hads on Ni within SS [33]. Although cathodic reduction of explosives can occur at lower potentials to avoid H₂ gas bubbles covering surfaces [36], kinetic rates may be slower. Higher potentials should increase reduction rates of explosives, which is needed in plug flow reactors when shorter hydraulic retention times in cathode regions are present when faster flow rates of treatment are desired. Higher operating potentials consequently produce H2 and alkaline conditions, which could be harnessed as side reactions for further explosives degradation in addition to direct electron transfer at cathode surfaces.

Therefore the objective of this work is to evaluate the use of SS to promote RDX, DNAN, and NQ degradation by three cathodic processes: direct electron transfer, reduction by H_{ads} , and alkaline hydrolysis. The SS composition and configurations are evaluated with the goals to maximize explosives removal and to minimize time to steady-state removal conditions. RDX is chosen because it is a commonly manufactured explosive, and DNAN and NQ are chosen as representative new IHEs. The three are expected to have different susceptibilities to the three cathodic processes owing to their different structures—RDX a cyclic nitroaliphatic, DNAN a nitraromatic, and NQ a nitroaliphatic with a C—N structure.

2. Materials and methods

2.1. Explosives

All chemicals used in this study are analytical grade. RDX used for

calibration was purchased from Sigma Aldrich or Lawrence Livermore National Laboratory. RDX used in experiments was synthesized through direct nitrolysis of hexamethylenetetramine (HA), [37] HA was incrementally added to stirred fuming nitric acid within an ice bath to keep the reaction temperature below 11 $^{\circ}\text{C}.$ The solids were filtered, rinsed with cold water, and then dried. To purify the solids and remove trace HMX, the solids were dissolved in acetonitrile at room temperature, filtered to remove any insoluble matter, and re-precipitated by addition of DI water to a composition of 33% water, 67% acetonitrile. After drying, the solids were confirmed to contain only RDX according to HPLC-UV and LC-MS-MS measurements. NQ was purchased from Sigma Aldrich. DNAN was purchased from Santa Cruz Biochemicals. DAAN was purchased from Sigma Aldrich. Deionized (DI) water (18.2 $\text{M}\Omega\text{-cm})$ obtained from a Millipore Milli-Q system was used in all the experiments.

2.2. Wire meshes

Titanium/mixed metal oxide (Ti/MMO, 3 N International) mesh was used in all experiments as an anode (3.6 cm diameter and 1.8 mm thickness). Different types of stainless steel woven mesh were evaluated as cathodes, including stainless steel wire cloth grades 304 (mesh number 20), 316 (mesh numbers 10, 20, 40, 60, 80, and 100), and 430 (mesh number 20) (all purchased from McMaster-Carr). Stainless steel 330 (mesh number 10) was purchased from Belleville Wire Cloth Co. Nickel alloys included acid-resistant 400 nickel wire cloth (McMaster-Carr), Nickel 200 (Belleville), Nichrome V (Belleville), iron-nickel foam (70%Ni, 30% Fe) (Xiamen Tmax Battery Equipments Limited), and nickel foam (99.99% Nickel) (MTI Corporation). These materials were cut into 42.3 mm diameter disks, and their physical properties are listed in Table 1. A complete list of chemical composition appears in Table S1.

It is noted that H2 gas evolution was observed on all cathodes and at all currents in this study. To support this observation, a linear sweep voltammetry curve for one representative SS wire mesh was referred to, which confirmed adequate electron transfer to oxygen-saturated sodium sulfate electrolyte solution at potentials lower than about -100 mV vs. SHE [38]. Here, the cathode potential of SS 316 wire mesh was checked at typical applied currents of 100 and 150 mA in our plug flow setup with oxygen saturated sodium sulfate solutions containing RDX, NQ, and DNAN. These cathode potentials were found to be even lower, between -150 and -250 mV, able to support hydrogen generation. These potentials were measured using a lithium acetate reference electrode (Nico2000) placed ~1 cm from the bottom of the cathode and connected to the multimeter and cathode via a pH/ORP/ion transmitter. The cathode potential was calculated as the measured potential difference between the solution and cathode, and these values were corrected to the standard hydrogen electrode scale by adding 0.2046 V.

2.3. Experimental setup

The plug flow electrochemical cell consisted of all electrodes within a vertical acrylic column reactor (208 mL), a direct current (DC) power source, and a peristaltic pump for maintaining constant flow (Fig. 1). Several disks were stacked together to produce the desired cathode length. Disks were connected to the DC power source via titanium rods within Teflon sleeves to prevent cathode-anode contact. Each experiment began by pumping the synthetic contaminated water upwards, and when filled, a fixed current was applied (potential was allowed to vary to maintain the fixed current). H_2 gas bubbles and O_2 gas bubbles were observed to form on the cathode and anode, respectively, for all applied currents. Experiments were conducted with high concentrations of either of three explosives (20–30 mg L^{-1}) with 5 mM Na_2SO_4 in order to determine the efficiency of the designed reactor with different cathode on the removal of RDX, NQ, and DNAN.

A split cell batch reactor was also used to test RDX, NQ, and DNAN reaction with the cathode or anode separately. Two glass cells were

Table 1 Physical properties of materials used for cathodes.

Material	Ni (%)	Mesh number (n)	Wire diameter (cm)	Pore size (cm)	Open area (%)	Calculated surface area (4 disks) (cm ²)	Average Weight per Discs (g)
Stainless steel							
430	0.75	20	0.041	0.086	46	108.4	2.14
304	9.25	20	0.041	0.086	46	108.4	2.04
316	12	10	0.064	0.191	56	90.3	2.61
316	12	20	0.041	0.086	46	108.4	2.17
316	12	20	0.046	0.081	41	119.8	2.55
316	12	20	0.058	0.069	29	149.6	4.13
316	12	40	0.025	0.038	36	124.3	1.54
316	12	60	0.028	0.014	12	192.0	3.15
316	12	80	0.015	0.018	19	176.6	1.66
316	12	100	0.015	0.011	30	146.8	0.84
SS904L	23-28	20	0.040	0.086	46	108.4	2.14
Nickel alloy							
Nichrome	60	20	0.041	0.086	46	108.4	2.05
Acid-resistant 400	63	20	0.041	0.086	46	108.4	2.31
Nichrome V	73.87	20	0.033	0.094	54.8	88.5	1.61
Nickel 200	99	20	0.036	0.091	51.8	94.9	1.97

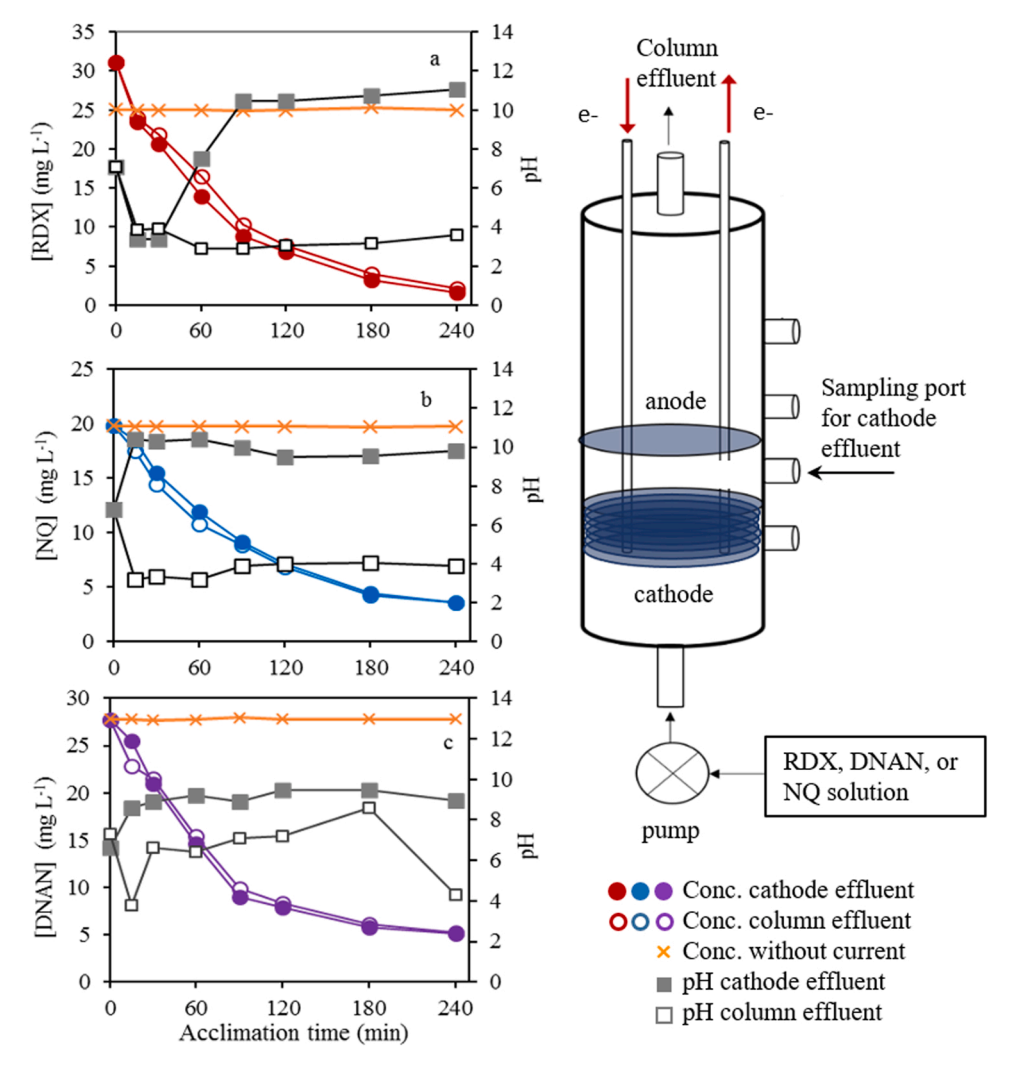


Fig. 1. Degradation of three explosives (a) RDX, (b) NQ, and (c) DNAN, using a SS 316 cathode. Filled circles are concentrations after cathode effluent, open circles are concentrations after column effluent (after anode), filled squares are pH after cathode effluent, open squares are pH after column effluent, and x symbols are concentrations without current applied. Initial conditions: 100 mA current, 4 disks, $2.0 \pm 0.1 \text{ mL min}^{-1}$ flow rate, 15 min hydraulic retention time, $\sim\!25~\text{mg L}^{-1}$ initial RDX, NQ, or DNAN concentration. The schematic on the right is of the electrochemical flow-through reactor with an upstream cathode and upstream anode. Electrodes were attached to titanium rods and connected to a DC power source.

joined by a proton exchange membrane (Nafion 212), with the cathode cell containing 5 disks of SS grade 316 (#80 mesh) and the anode cell containing 5 disks of Ti/MMO mesh. Disks were attached via titanium rods to a DC power source. Experiments were conducted with either of three explosives (20–30 mg $\rm L^{-1})$ with 50 mM Na₂SO₄—a higher salt

concentration was needed to keep potential sufficiently low for the fixed current of 150 mA.

2.4. Analytical methods

Aqueous samples from the cathode effluent and the column effluent were analyzed for the parent explosive compounds using an Agilent 1260 Infinity Series high-performance liquid chromatography (HPLC). All liquid samples were filtered through a 0.22 μm nylon filter. 1 mL of sample was then preserved by addition of 0.1 mL of 100 mM phosphate buffer (pH 7.0) to decrease the pH and avoid alkaline conditions during storage. A 20 μL sample was injected into a Supelco LC-18 column (C-18 reversed-phase HPLC column, 15-cm) with a mobile phase of 50/50 (v/v) methanol/organic-free reagent water. The flow rate was 1 mL min and UV detector set at 254 nm for all explosives. RDX, NQ, DNAN, and DAAN were identified by retention time using standard solutions.

Organic degradation products of RDX and NQ were identified using LC-MS-MS. High sensitivity quantitative measurements and non-target screening was performed using a QTrap 4500 (AB Sciex) mass spectrometer paired with a Shimadzu Prominence HPLC system. The curtain gas pressure was set to 20 psi, the IonSpray voltage was set to - 4500 V, the source temperature was set to 360 °C, GS1 (nebulizer gas pressure) was set to 60 psi, and the GS2 (auxiliary gas pressure) was set to 60 psi. Separation was performed with a Hypersil Gold PFP column (Thermo Scientific, 2.1 mm x 100 mm, 3 µm) using 10 mM ammonium formate in water and 10 mM ammonium formate in methanol as the mobile phases at a combined flow rate of 0.5 mL min⁻¹. For targeted analysis a gradient was run from 35% methanol to 98% methanol over 6.8 min. For nontargeted analysis a gradient was run from 2% methanol to 98% methanol over 22 min. The first two minutes of chromatography eluent were wasted to avoid injection of the Na+ and SO_4^{2-} salts into the MS. This instrumentation allows for first tracking for candidate compounds using a narrow m/z range (+/- 0.3 Da around the compound molecular weight or anticipated adduct) in a chromatogram. Candidate compounds are reported only if the candidate was reported elsewhere in the literature, if a peak in a chromatogram was obtainable, if the peak signal is found in reactor samples, and if no peak signal can be found in reactor blanks or initial test solutions.

Inorganic degradation products nitrite, nitrate, acetate, and formate were measured by ion chromatography (Dionex DX-120 with 9 mM Na₂CO₃ eluent at 1.5 mL min⁻¹ through an AS9-HC column), and ammonium was measured using an ammonium probe (Orion High Performance Ammonia Probe). A portable pH/ORP/Temperature meter (Orion Star A221) was used to measure pH.

Possible leaching of metals from the Ti/MMO, SS 316, and nickel foam electrodes during operation was checked by measuring aqueous samples using an inductively coupled plasma – mass spectrometer (Bruker Aurora M90, serviced by Analytik Jena).

The surface oxygen functional groups and iron speciation were identified by X-ray photoelectron spectroscopy (XPS) using a Surface Science Instruments X-probe SSX-100 (Cornell Center for Materials Research Shared Facilities). Samples were mounted on carbon tape. Survey scans (150 eV pass energy) were taken of the samples as received, but the samples were then cleaned using an Ar ion gun (4000 eV, with a 3 μA current for 30 s) prior to high resolution Fe2p and O1S scans collected at 50 eV. Spectra were analyzed with CasaXPS software and fit with Gaussian-Lorentzian peak shapes after a Shirley background correction.

Images of SS grade 316 wire meshes (mesh size #80) were taken using scanning electron microscopy (SEM, FEI Scios DualBeam), and elemental analysis was performed with energy dispersive spectroscopy (EDS, Oxford Instruments).

3. Results and discussion

3.1. Electrochemical dynamics of RDX, NQ, and DNAN removal

RDX, NQ, and DNAN all decrease in concentration after passing through the cathode when 150 mA current is applied (Fig. 1). No

explosives removal occurs when current is off, indicating explosives removal is likely due to a redox reaction, and losses of the compounds to sorption on surfaces or volatilization are not likely. The removal appears to occur in the cathode only because there is no further removal of each explosive after the anode. To further test this idea, a split cell batch reactor was used to monitor RDX, NQ, and DNAN separately at isolated cathode and anode cell. Only trace RDX degradation (~1 mg L-1), and no NO or DNAN degradation, were found to occur within the anode cells, and degradation of these explosives was confirmed within the cathode cell (Fig. S1). Therefore compound removal is likely due to reduction reactions caused by the cathode, consistent with previous reports for cathodic reduction of these explosives [17,18]. Although significant RDX oxidation on Ti/MMO anodes is possible [19,39], the absence of anodic reaction observed here could be due to different anode material properties, unfavorable voltage, hydraulic retention time, or solution pH.

The separate cathode and anode also created two distinct zones of pH caused by water electrolysis. The increase of pH right after the cathode is due to OH⁻ production as part of the water electrolysis reaction:

$$2H_2O + 2e^- \rightarrow H_2(g) + 2OH^-$$
 (1)

Whereas the pH decrease after anode is due to H⁺ production:

$$2H_2O \rightarrow O_2(g) + 4H^+ + 4e^-$$
 (2)

Flowing through the unbuffered explosives solutions resulted in pH 9–11 in the cathode and pH near 4 after the anode. The creation of alkaline pH conditions might create an environment for alkaline hydrolysis reactions to contribute to explosives removal, as discussed below.

The dynamics of explosives removal and pH changes show that an acclimation time is needed to reach a steady-state electrochemical condition. Interestingly, only 10–60 min is typically needed for pH values to stabilize, but explosives removal requires up to 4 h, as previously observed for TCE removal in a similar reactor setup [33]. Note that the hydraulic retention time in the 4-mesh cathode zone is 15 min at this flow rate, and so after 4 h acclimation time, 81–95% of the explosives in Fig. 1 are removed within this hydraulic retention time. This concentration versus acclimation time profile was found to be reproducible over triplicate experiments for RDX, NQ, and DNAN (Fig. S2). In the sections below, cathode materials and operating conditions are then optimized to decrease acclimation time and improve removal extent.

3.2. Influence of cathode material on RDX, NQ, and DNAN removal

Several grades of SS were evaluated to test the possibility that chemical composition of cathode materials could influence explosives removal. The best-performing SS material for RDX and NQ removal (Fig. 2) is SS grade 316, which showed a faster approach to steady state and greater removal extent in this 4 h of acclimation time compared to other SS meshes. Some SS and Ni alloys produced far less removal extent of RDX and NQ.

To possibly explain the differences in cathode performances, the Ni content was hypothesized to participate in reduction by providing surfaces for H_{ads} , an idea proposed previously for TCE reduction by SS cathodes [33]. The catalytic hydrogenation reaction by H_{ads} preferentially occurs at alkene or C=N bonds, so NQ's central C=N structure could make it susceptible to hydrogenation. In fact, Ni % does trend well for NQ removal with SS cathodes, specifically SS430 (0.8% Ni) < SS304 (9.25% Ni) < SS316 (12% Ni). SS904L with the highest Ni (22.5%), though, does not continue improved performance with NQ, but this material could actually be discounted because it contains an intentional corrosion resistant coating (i.e., addition of Mo and more Cr for Cr oxide formation) which could block access to Ni surface sites. Ni % also trends well with NQ removal extent for all Ni alloys according to Nicrome (60% Ni) < acid resistance 400 (74% Ni) < Nichrome V (74% Ni) < Nickel

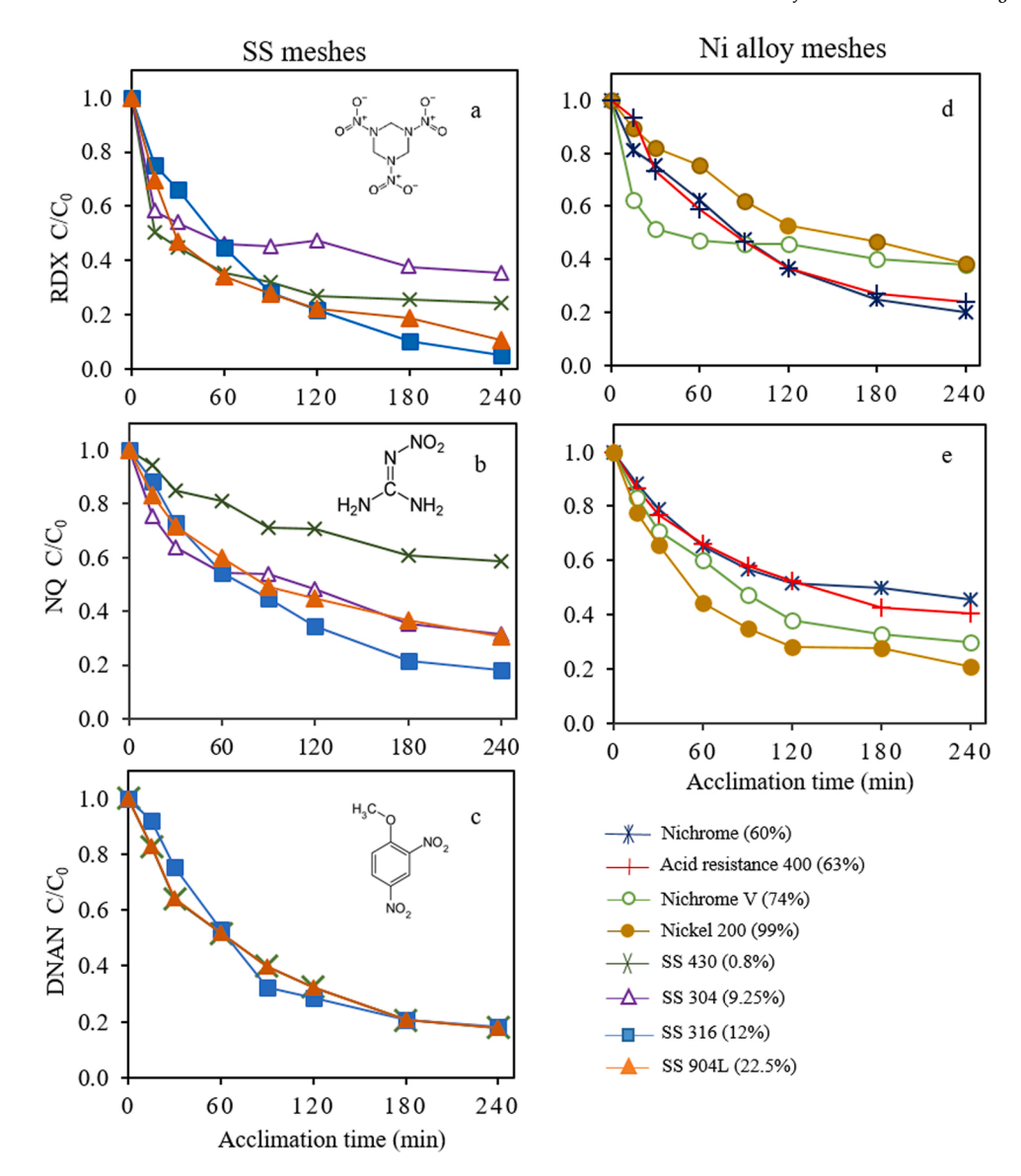


Fig. 2. Degradation of three explosives (a) RDX, (b) NQ, or (c) DNAN, by different SS cathodes with different Ni percentages, and degradation of two explosives (d) RDX and (e) NQ by different Ni metal or alloy cathode materials. Values in parentheses are Ni percentages. Initial conditions: 100 mA current, 4 disks stacked, 2.0 \pm 0.1 mL min⁻¹ flow rate, 15 min hydraulic retention time, ~25 mg L⁻¹ initial RDX, NQ, or DNAN concentration.

200 (99% Ni). No other trend in elemental composition with NQ removal was apparent.

Despite also showing a modest range in removal extents on different cathode materials, RDX removal extent did not trend with Ni % or any other element abundance. RDX does not have any double-bonded structures within its heterocyclic ring and therefore is not an ideal probe compound for testing hydrogenation. The variability in performance might be attributed to that RDX, after an initial reduction step, is susceptible to ring breakdown via a few different pathways, which might be sensitive to slightly different environments created by different cathode materials.

Similarly, a higher Ni % in SS does not increase DNAN removal, and in fact DNAN removal was invariant among all four SS grades (Fig. 2). As the only reduction reaction of DNAN is reduction of the nitro groups to amine groups [40–42], it appears any H_{ads} also does not significantly influence the nitro-group reduction reaction under the reaction conditions here (alkaline pH, SS surfaces, hydraulic retention time 15 min). Catalytic hydrogenation, though, can reduce nitro groups on benzene molecules under harsher conditions. Nitrobenzene can be reduced rapidly using noble metal catalysts at higher temperatures and either in

the gas phase or in organic solvents, both with ample hydrogen gas or borohydride provided as an H source [43,44]. H_{ads} on graphite was inferred to be responsible for 2,4-dinitrotoluene reduction in aqueous solution, but this reaction required a few hours for completion [45]. H_{ads} also would not break aromatic C-C bonds. The process of direct electron transfer at the cathode surface is likely the sole transformation pathway for DNAN, as well as the primary transformation pathway for RDX and NQ.

Despite Ni alloys having far greater Ni content than the SS grades, no Ni alloy performed superior to SS316. It is possible that corrosion protection coatings of the Ni alloys also limits H_{ads} formation and presence as a secondary reductant, if any. SS316 would be the preferred cathode material over 99% pure Ni due to similar performance but at much lower material cost. Overall, the superior performance of SS316 could possibly be explained by less protective coatings and a minor amount of additional Ni.

3.3. Influence of cathode surface area on RDX removal

The SS316 material was further optimized considering its geometric

properties, specifically investigating ways of increasing surface area to improve performance with RDX (Fig. 3). For one, increasing the number of disks increased the reactive surface area, lengthens the cathode, and increases contact time. Increasing the number of disks from 4 to 15–30 did have a positive effect on shortening the acclimation time. While 30 disks did decrease acclimation time, after 4 h, all removal extents were nearly the same no matter the cathode length. There are two possible reasons for similar performance at 4 h. One is that, after 4 h acclimation time, the current and potential are not distributed homogeneously throughout the cathode, but rather more greatly concentrated at the cathode end nearest to the anode. Such a current distribution would lessen the usefulness of longer cathode lengths. Second, more bubble accumulation below the stacked disks was observed with increasing number of disks stacked, which might have limited some surface area exposure to RDX [33], at least near the cathode inlet.

Higher mesh numbers give more wires per area and consequently more surface area, which was expected to improve RDX removal extent through more contact between RDX and the cathode. However, increasing mesh number did not result in any definitive trend in RDX removal (Fig. S3). The highest mesh (#100) behaved as poorly as the lowest (#10), which could be due to slower bubble release on the disks which limits exposed surface areas, or possibly more flow restriction through the smaller pores which also limits contact between RDX and all surfaces. Despite a lack of trend with mesh size, mesh #80 did show the shortest acclimation time and was therefore identified as the optimal mesh number.

Finally, RDX removal extent is insensitive to wire diameter when tested at the same mesh number, despite a 38% increase in provided surface area when increasing diameter from 0.041 cm to 0.058 cm (Table 1). In fact, RDX removal percentage after 4 h did not correlate at

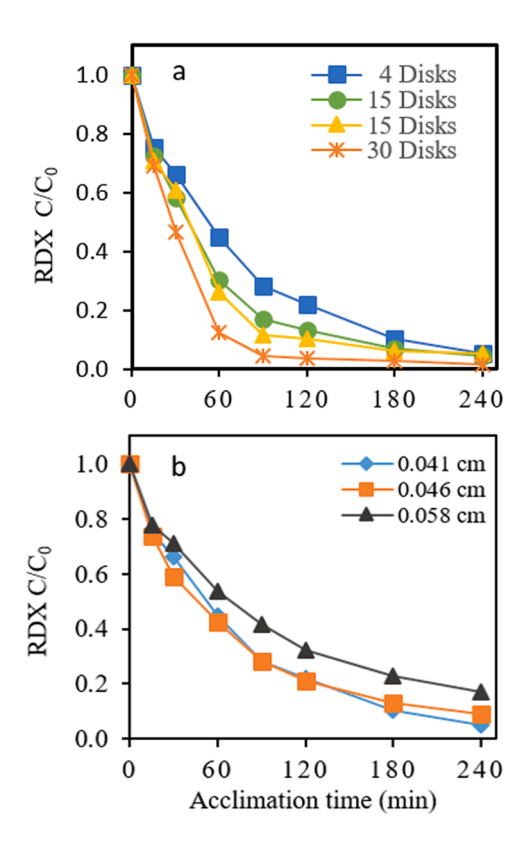


Fig. 3. Influence of different cathode surface areas on removal extent of RDX using SS316 disks by way of varying disk number (a) or wire diameter with 4 disks (b). Initial conditions: 100 mA current, 2.0 ± 0.1 mL min⁻¹ flow rate, \sim 25 mg L⁻¹ RDX concentration. Hydraulic retention times were as follows: 15 min for 4 disks (in panels a and b), 18 min for 15 disks, and 25 min for 30 disks.

all with the calculated surface areas across all SS316 experimental variations (data not shown). It is possible surface bubble accumulation and preferential flow paths cause performance to be less predictable by cathode surface area. The more important geometric considerations for design with these wire meshes appears to be the cathode length and the empirically observed optimal pore size with mesh #80.

3.4. Role of alkaline hydrolysis

Alkaline hydrolysis can contribute to explosives degradation within electrochemical systems provided sufficient contact time and pH [20]. In Fig. 1, cathodic pH varied in the range of 9–11.5. Because homogeneous degradation of the explosives could occur by this secondary process with OH, the contribution of alkaline hydrolysis to removal extents was estimated using an experimentally-derived kinetic model for each explosive. Alkaline hydrolysis rates of RDX, NQ, and DNAN were individually measured in batch at pH 10–14 adjusted by addition of NaOH (Fig. 4a-c). For pH values below 11 or 12, only minor or modest amounts of RDX< NQ, and DNAN were degraded, showing alkaline hydrolysis may be less important as a potential degradation process. Higher pH results in faster removal rates, and at pH 14 for RDX, 20 mg L-1 RDX was completely degraded in about 15 min.

Hydrolysis profiles of RDX, NQ, and DNAN at each pH > 11 could be modeled with the pseudo-first-order decay model (Eq. 3). The reaction order of 1 with respect to explosive concentrations C_b was confirmed (model fits appear in Fig. S4).

$$\frac{dC_b}{dt} = -k_{obs}C_b \tag{3}$$

In order to find the reaction order with respect to $OH^-(\beta)$ concentration and an intrinsic reaction rate coefficient (k_{OH}), the pseudo-first-order coefficient k_{obs} was expanded as

$$k_{obs} = -k_{OH}|OH^-|^{\beta} \tag{4}$$

And linearized to Eq. 5 to derive k_{OH} and β from the intercept and slope, respectively.

$$\log k_{obs} = -\log k_{OH} + \beta \log[OH^{-}]$$
 (5)

Almost no changes in pH values before and after reaction were observed under these conditions (Table S2), and [OH] values were considered constant. Plotting $\log k_{obs}$ values versus $\log[OH^{-}]$ showed good linear correlation between pH 12-14 for all three explosives (Fig. 4d-f). Reaction orders with respect to [OH-] were close to firstorder for RDX and DNAN. Alkaline hydrolysis kinetics of RDX and DNAN were previously described as first order with respect to both the explosive and OH concentrations [12,13,46,47]. The reaction order of 0.56 with NQ, though, points to a more complicated reaction mechanism with OH^- than just a biomolecular reaction. The intrinsic k_{OH} value for DNAN observed here (0.04–1 min⁻¹) is nearly identical to previously reported value of 0.043–1 min⁻¹ [12]; however, our pH-specific k_{obs} values are 4- to 11-fold different from others (0.0004 min⁻¹ vs. 0.0058 min^{-1} [43], and 0.004 min^{-1} vs. 0.0012 min^{-1} [13]. k_{OH} for RDX at room temperature here (0.56–1.17 min⁻¹.17) is an order of magnitude smaller than the closest temperature reported in the literature at 50°C $(6.35-1 \text{ min}^{-1})$ [46] k_{OH} for NQ was the lowest of the three explosives with 0.01-1 min⁻¹.

The kinetic models can help estimate the contribution of alkaline hydrolysis to explosives degradation. k_{obs} values can be calculated for expected cathodic conditions, specifically that the pH values can approach 12 and an exposure time of 45 min (through the cathode and the gap before the anode). These conditions would predict alkaline hydrolysis could decrease RDX, NQ, and DNAN initial concentrations by 11%, 3%, and 2%, respectively.

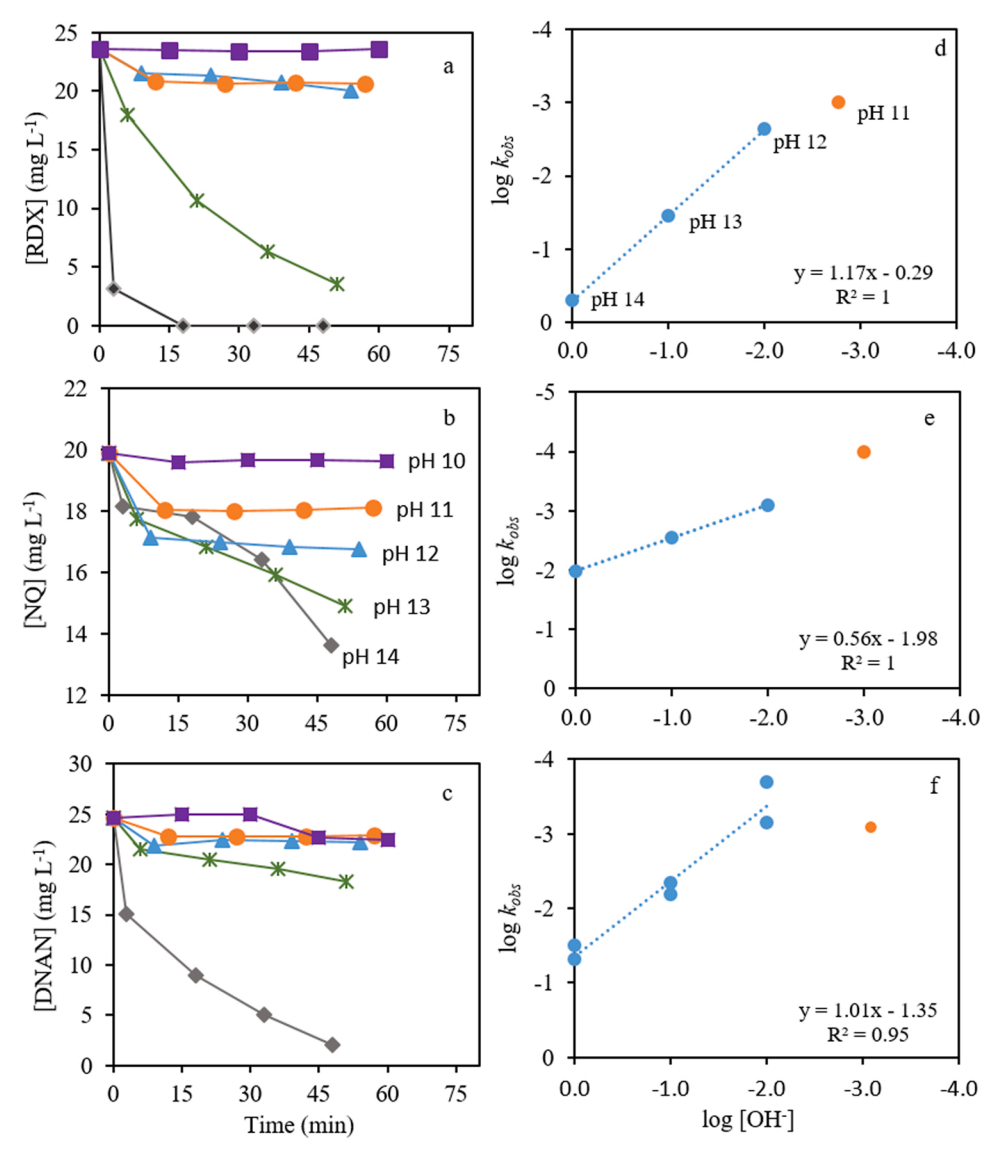


Fig. 4. Degradation of (a) RDX, (b) NQ, and (c) DNAN over time by alkaline hydrolysis within batch reactors at different pH. Data fits to pseudo-first order rate expressions appear in Fig. S4. Correlations between $\log[\mathrm{OH'}]$ and $\log k_{obs}$ according to Eq. 5 appear for (d) RDX, (e) NQ, and (f) DNAN. Only pH 12–14 are included in the correlation due to minimal removal observed at pH 10 and 11. For DNAN, a second set of kinetic batch reactors were conducted for pH 12–14 for reproducibility, and their $\log k_{obs}$ values are plotted in (f) alongside those from panel (c).

3.5. RDX, NQ, and DNAN degradation products

Commonly reported degradation products of each parent explosive were explored for in order to better understand degradation pathways occurring within the column reactor. Aqueous samples were taken from the column effluent once the 4-h steady state condition at 150 mA was reached, and candidate compounds were sought for using LC-MS-MS. All chromatograms of detected compounds, their conditions of measurement, and their structures are provided in Fig. S5.

The candidate compounds found for RDX, and therefore considered to be possible reaction intermediates here, include MNX (hexahydro-1-nitroso-3,5-dinitro-1,3,5-triazine) and MDNA (methylenedinitramine), both of which have been observed in electrochemical reductive systems and raise concerns of enhancing toxicity of the effluent [17,19,22]. While the nitroso derivative is indicative of nitro-group reduction, MDNA is a ring cleavage intermediate that could form via different degradation routes including one initiated by reduction to MNX or direct cleavage of RDX [48]. Interestingly, the compound N,N-dinitroaminol was also observed in the electrochemical column effluent, and this compound forms when a hydroxyl group replaces an H on a C in RDX. N, N-dinitroaminol was reported as an oxidation product after reaction with permanganate [49], and it is possible that the anode was responsible for a small amount of RDX oxidation to N,N-dinitroaminol here.

Ammonium, nitrite, and nitrate were quantified and collectively accounted for 31% of reacted N from parent RDX. Ammonium and nitrite confirm the N-N bond is cleaved, and both have been observed in systems transforming RDX by reductive and oxidative means [50-52]. The presence of nitrate suggests some oxidation of N species at the anode surface in order to acquire its third O. The anode surface may well provide oxidative conditions for oxidizing intermediate compounds. Formate and acetate accounted for 42% of reacted C from RDX. Formate and acetate were observed in alkaline hydrolysis reactions [20,46], though it is possible some separate electrochemical reactions were responsible for its formation, in particular the conversion of dissolved CO₂ and formate to acetate through some radical intermediates [53]. It is possible other small organic C and N degradation products co-eluted with the background electrolyte and were lost to waste. Gaseous or volatile products such as N2O and HCHO may have been lost by stripping by H₂ or O₂ bubbles.

The reduction product nitrosoguanidine was observed during treatment of NQ and confirms some nitro group reduction occurred to a nitroso group. Moreover, nitrourea was also detected, and this compound could have formed by oxidation of NQ at anode surfaces because it has been identified as a NQ degradation product in aerobic microbial systems [54]. Ammonium, nitrite, and nitrate concentrations together accounted for 21% of the reacted N, and formate and acetate collectively

accounted for 28% of reacted C. These mineralized products indicate cleavage of the N-N, C=N, and C-N bonds.

The sole product of DNAN transformation tentatively identified here was 2,4-diaminoanisole (DAAN), formed by reduction of both nitro groups of DNAN. DAAN was confirmed by HPLC-UV retention times, and the brown color of DAAN was immediately noticeable in the cathode effluent. DAAN was previously identified as a DNAN reduction product in anaerobic microbial systems [55] and reductive systems featuring iron [42]. The cathodic processes did not cleave the aromatic ring to smaller organic or inorganic products under these conditions.

3.6. Influence of applied current and flow rate on RDX removal

Applied current and flow rate were adjusted to understand a practical range of operating conditions. A cathode comprised of a stack of thirty disks of SS 316, #20 mesh, was tested with RDX solution at 100,

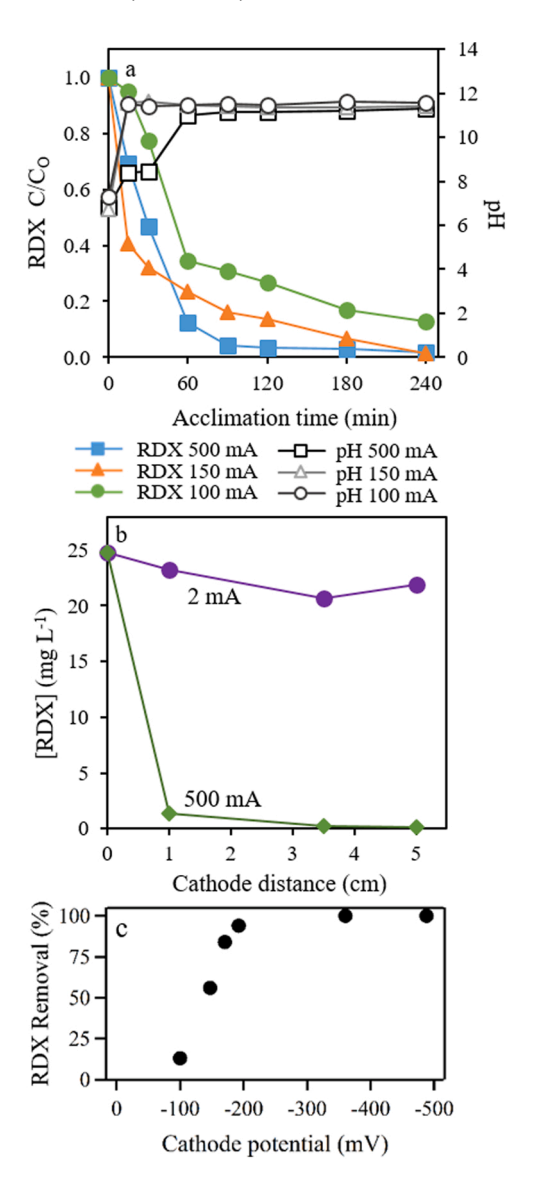


Fig. 5. (a) The influence of different currents (100 mA, 150 mA, 500 mA) on time to steady state condition for RDX degradation using SS 316 cathode (mesh #20, 30 disks stacked). (b) RDX concentrations over cathode distance at two different currents (2 or 500 mA). (c) RDX removal % at cathode effluent after 4 h acclimation time for different cathode potentials. Filled symbols are cathode effluent RDX concentrations, and open symbols are pH values. Initial conditions: flow rate 2.0 ± 0.1 mL min $^{-1}$, hydraulic retention time 25 min, \sim 25 mg L $^{-1}$ RDX concentration.

150, and 500 mA, and cathode effluent RDX concentrations and pH were monitored (Fig. 5a). The RDX removal extent clearly increased after 60 min acclimation time with increasing current. Higher current giving greater removal efficiency has been confirmed in previous studies treating RDX in a flow-through cell [17]. After 4 h acclimation time, though, complete RDX removal in the effluent was observed for both 150 and 500 mA. While 500 mA did provide the advantage of a much shorter acclimation time and achieved steady-state removal by 2 h, this current also increased the effluent temperature to 40°C. An applied current near 150 mA is effective, has less energy consumption, and has greater degradation efficiency, if a 4 h acclimation time can be tolerated. Cathode effluent pH reached to almost 12.0 for all currents. Interestingly, the time to steady-state pH values was much shorter than that for RDX concentrations, with $<15\,$ min required at 100 and 150 mA.

RDX concentrations were also sampled along the length of the cathode after 4 h acclimation time, and a comparison is made between two extreme values of current (2 mA and 500 mA). The concentration profile at 500 mA shows that nearly all RDX is removed within the first cm of the cathode length, and RDX removal to below detection limits was possible by the cathode effluent. This result, as well as the results from Fig. 3, illustrate that longer cathodes can be exploited for increased RDX removal by providing more contact time between RDX and cathode surfaces. Minimal current (here, 2 mA) is insufficient for any RDX removal with SS cathodes. Other cathode materials, though, e.g. reticulated vitreous carbon [17], have been reported as supporting RDX removal at low currents (10 mA).

To better identify an optimal applied current value, additional experiments were performed with varied currents and consequently cathode potentials, and RDX removal extents were measured at the cathode effluent after 4 h acclamation time. As described above, higher currents may improve RDX removal extent, but there may be a point where additional current either interferes by H2 bubble production or becomes wasteful. Plotting RDX removal extents versus cathode potentials (Fig. 5c) shows two distinct regions of behavior. RDX removal extent increases somewhat linearly as cathode potential increases at first from about -100 mV to about -200 mV (corresponding to about 2-150 mA). This region represents an electron transfer limitation on reaction rate, where additional current does lead to greater RDX reduction. The second region is a plateau where RDX removal extent flattens at a maximum of 100% at potentials greater than about -200 V. Here, mass transfer of RDX to the surface is limiting the reaction rate, that is, the rate is limited by how fast RDX can diffuse to the cathode surface. A cathode potential of about -200 mV (or an applied current of about 200 mA) where 100% removal of RDX is reached after 4 h acclimation time, can therefore be identified as an optimal operating condition. Lower applied voltages or currents do not produce as high of removal extent as could possibly be achieved. At lower applied voltages, it is still possible that H2 bubble accumulation at the cathode could be preventing some cathode surface exposure, but there is a clear benefit to increasing applied voltages to near -200 mV where RDX reduction can overcome any H₂ bubble interference and be completely removed. Higher voltages above -200 mV do not improve RDX removal and instead could produce negative impacts including energy wasted, energy lost as heat, and additional H_2 bubble formation and accumulation.

The RDX solution flow rate was also adjusted to explore whether RDX removal extent could be sustained at higher flow rates and consequently shorter cathode hydraulic retention times. Increasing the flow rate from 2 mL min⁻¹, to 5 mL min⁻¹, to 10 mL min⁻¹ did decrease RDX removal from 98%, to 84%, to 50%, respectively (Fig. 6). As expected, complete RDX removal would be better sustained at slower flow rates. In addition, these observations provides some insight to how RDX removal behavior can be modeled in this cathodic system. Specifically, it was assumed that the cathode could be modeled as a plug flow reactor, that pseudo-first order RDX degradation kinetics $C = Coe^{-kt}$ apply, and that the measured RDX effluent concentrations represent the concentrations C

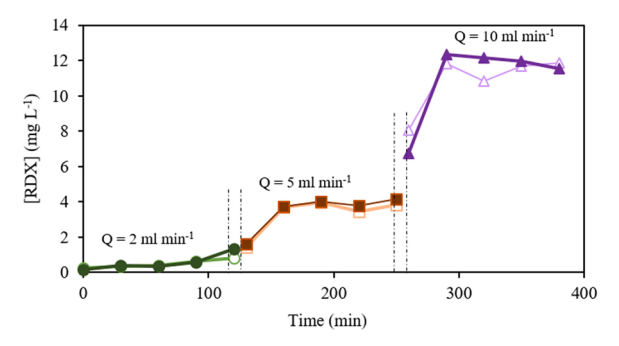


Fig. 6. The influence of different flow rates $(2.0\pm0.1~{\rm mL~min}^{-1},~5.0\pm0.1~{\rm mL~min}^{-1},~10.0\pm0.1~{\rm mL~min}^{-1})$ on cathodic degradation of RDX. Filled symbols are RDX concentrations in the cathode effluent, and open symbols are RDX concentrations in the anode effluent, which again show no anodic degradation of RDX. Vertical dashed lines indicate the brief time the flow rate was switched to a new value which required a few minutes of adjustment. Initial conditions: 4 disks of SS316 wire meshes, 100 mA current, ~25 mg L⁻¹ RDX. Corresponding hydraulic retention times were 15.2, 6.2, and 3.1 min.

after cathode hydraulic retention time t. To check if reaction kinetics at the cathode were consistent at different flow rates, k was calculated at each hydraulic retention time 15.2 min, 6.2 min, and 3.1 min for flow rates of 2 mL min⁻¹, to 5 mL min⁻¹, to 10 mL min⁻¹ respectively. Similar k values of 0.27 min⁻¹, 0.29 min⁻¹, 0.30 min⁻¹ were obtained for these three different flow rates. Reaction kinetics are therefore unchanged with this range of flow rates, and it is possible to model RDX effluent behavior with a simplified, overall first-order kinetic model while up to three simultaneous degradation processes occur.

Consequently, it is possible to relate flow rate, reactor configuration, hydraulic retention time, and reaction kinetics in one simple model. However, to predict reactor performance under different applied currents and solution conditions, a more complex model including relevant electrochemical system parameters is required. Electrochemical plug flow reactors treating dissolved organic pollutants have been described using Butler-Volmer kinetics which include rate coefficients at cathode surfaces and solution overpotentials for specific pollutants and water chemistries [34]. With the optimized cathode material determined here, future experiments will take a similar modeling approach to capture intrinsic cathodic process behavior to multiple explosives compounds under flow-through conditions. Spatially resolved concentration and pH data along the cathode length will be particularly helpful to understanding the spatial distribution of cathodic processes and to estimating useful cathodic lengths.

3.7. Longevity of SS316 as cathode material

The longevity of SS316 for use as a cathode material was assessed first by an experiment comparing its performance in a new, unused state with performance after > 100 h operating use. RDX concentration versus acclimation time profiles were the same when either cathode materials were present, showing similar approaches to a similar steady-state condition (Fig. S6). The electrical properties therefore appeared unchanged after prolonged use. The chemical properties were also checked after use, first by measuring whether any metals were leached from the cathodes after use. Aqueous samples taken from the column effluent showed no detection of any Fe, Ni, Mn, Cr, or Ti. Stainless steels typically have some protective coating (some thicker or more chemically resistant than others), and under reductive conditions, chemical leaching was not observed.

To better quantify any surface changes, SEM-EDS measurements were taken for unused SS316 wire mesh and used SS316. SEM images showed the surface features rather unchanged after prolonged use (Fig. S7). The atom percentages from SEM-EDS spectra were averaged from five measurements on each sample and compared using the t-test

(alpha value of 0.5). Measured abundances for Fe, C, Ni, and some minor elements showed no significant statistical differences between the unused and used SS316 materials (Table S3). A slight increase in Cr abundance (15.9–16.4%) and a slight decrease in O abundance (1.3–0.9%), though, were statistically significant. One possible explanation is that the applied current reduced surficial metal oxides to elemental states and released O during operation.

As a test of the idea of metal reduction, XPS spectra were also taken to check any changes in Fe speciation (Fe being the more prominent metal in SS). First, broad survey spectra were not helpful in confirming surface elemental abundances or in obtaining high resolution spectra due to the presence of a thin film of carbon (Fig. S8). Accordingly, the C film was removed by an Ar ion stream, and high resolution Fe2p and O1s $\,$ spectra were obtained (Fig. 7). Fe⁰, Fe²⁺, and Fe³⁺ components were identified in both the $Fe2p_{1/2}$ and $Fe2p_{3/2}$ signal peaks, and their binding energies (Table 2) were similar to those found on stainless steel [56] and oxidized iron [57]. The relative abundances of the $Fe_{3/2}^0$ and Fe_{1/2} components increased after use, and concomitantly the relative abundances of all Fe²⁺ and Fe³⁺ components decreased. This observation supports the possibility that applied current partly reduced the oxidized Fe to elemental Fe. The O1s spectra did confirm the presence of O²-, OH⁻, and H₂O, but their relative abundances remained largely unchanged after use.

4. Conclusions

A flow-through electrochemical reactor with a separated cathode and anode was evaluated for degradation of three explosive compounds, RDX, NQ, and DNAN. Separating the cathode from the anode provides an advantage of localizing conditions for reductive degradation and alkaline hydrolysis processes supported by the cathode, compared to conventional stirred batch reactors with more homogeneous conditions. Reduction of RDX, NQ, and DNAN in the cathode region was confirmed, and nearly entire removal of each explosives (~25 mg L⁻¹) was accomplished within 15 min flow-through contact time. Batch reactors at varying pH were used to derive kinetic models for alkaline hydrolysis that were first-order with respect to explosive concentration and varying order with respect to hydroxide ion concentration. These models predict only < 11% of influent explosives could be removed by alkaline hydrolysis under the pH conditions observed in our plug flow system, with RDX the most susceptible to hydrolysis. The Ni content of SS is also hypothesized to possibly support adsorbed atomic hydrogen as a secondary reductant, but only for NQ which is more susceptible to catalytic hydrogenation.

Through testing several metal wire meshes, the best-performing cathode material for all three explosives was identified as SS grade 316, mesh number 80. However, some limitations on plug flow applications of wire mesh cathodes were also identified. For one, an acclimation time of up to 4 h, during which explosives are only partly removed, is required before steady-state removal conditions are reached. Longer cathode lengths, achieved by stacking more wire meshes, may help shorten the acclimation time. Second, the applied currents producing effective explosives reduction here also produced H2 gas bubble generation and accumulation at cathode surfaces, and their presence might limit surface contact with contaminants. Corrosionprotection coatings on SS could adversely affect the extent of explosives removal, and cathode material selection should avoid such coatings. Finally, higher currents can produce greater RDX removal extents and shorter acclimation times, but an upper limit of operation near 500 mA was determined based on excess heat generation, and a value near 200 mA may be more optimal. The results of this work serve as a basis for material design, optimized operating conditions, and practical considerations for larger scale reactors. Lastly, to complete the removal of possible toxic intermediate or product compounds formed after degradation by cathodic processes, a further treatment unit downstream of a reductive electrochemical reactor may be needed, such as those that

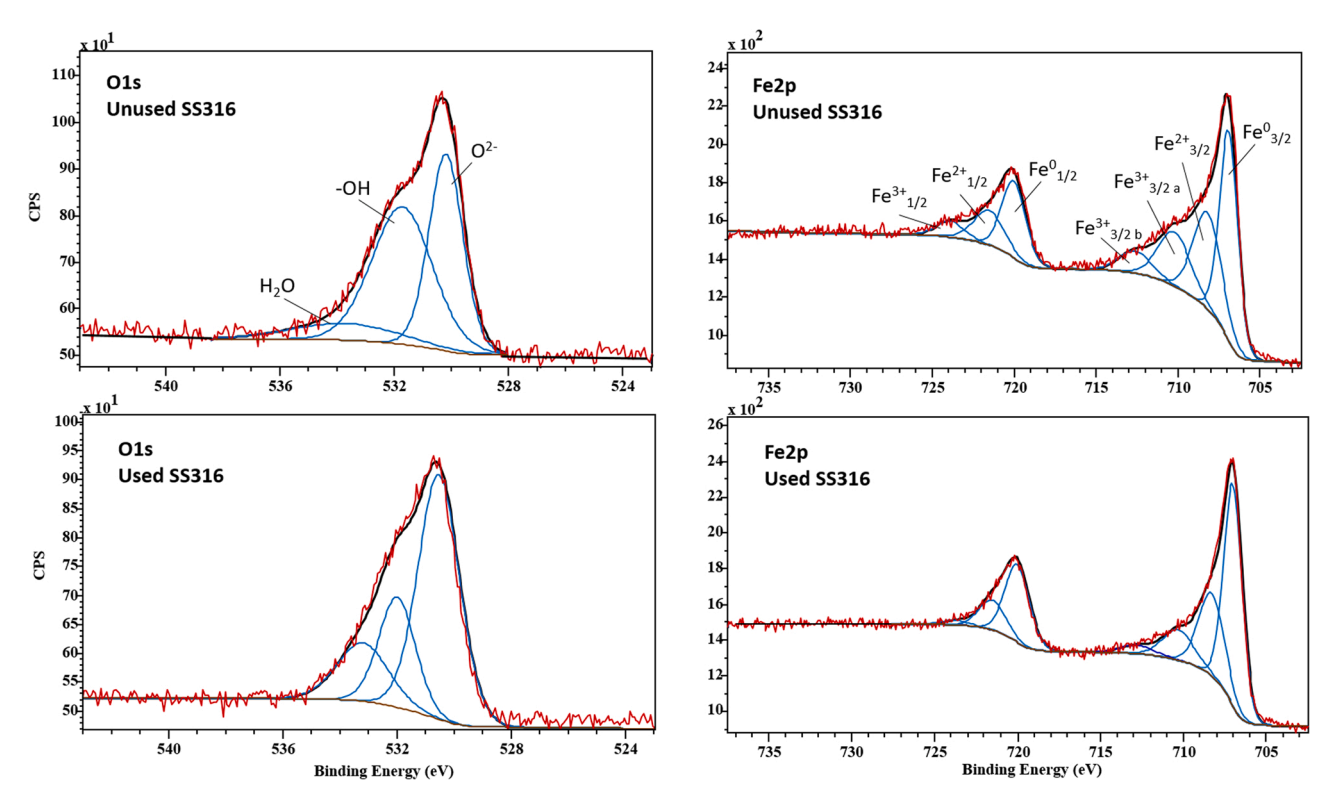


Fig. 7. High resolution XPS spectra of O1s and Fe2p for both unused (top two panels) and used (>100 h operating time, bottom two panels) SS316 wire mesh (#80). Spectra were collected after cleaning material surfaces with an Ar ion gun. The same component peaks labeled in the top panels are present in bottom panels, though may be at smaller proportions.

Table 2X-ray photoelectron spectroscopy fitted model parameters for unused SS316 and used SS316 wire meshes.

Unused SS316											
Fe2p				O1s							
	Binding Energy eV	Relative area %	FWHM		Binding Energy eV	Relative area %	FWHM				
Fe ⁰ 3/2	706.9	30.9	1.3	O ²⁻	530.3	57.9	1.6				
Fe ²⁺ 3/2	708.2	22.0	2.0	-OH	531.9	22.8	1.5				
Fe ³⁺ 3/2 3	710.2	14.2	2.3	H_2O	532.9	19.3	2.2				
Fe ³⁺ 3/2 b	712.6	5.8	2.3								
Fe ⁰ 1/2	720.0	15.0	1.7								
Fe ²⁺ 1/2	721.5	8.6	2.2								
Fe ³⁺ _{1/2}	723.9	3.6	2.0								
Used SS316											
C1s				O1s							
	Binding Energy	Relative area	FWHM		Binding Energy	Relative area	FWHM				
	eV	%			eV	%					
Fe ⁰ 3/2	707.0	39.9	1.3	O^{2-}	530.5	59.0	1.7				
Fe ²⁺ 3/2	708.3	20.5	1.8	-OH	532.0	23.5	1.5				
Fe ³⁺ 3/2	710.3	9.1	2.2	H_2O	533.1	17.5	2.1				
Fe ³⁺ 3/2	712.8	2.7	2.3								
Fe ⁰ 1/2	720.0	18.7	1.7								
Fe ²⁺ 1/2	721.5	8.0	1.9								
Fe ³⁺ 1/2	723.7	1.1	1.7								

utilize oxidation or adsorption reactions.

CRediT authorship contribution statement

Nazli Rafei Dehkordi: Investigation, Writing – original draft, Visualization. Michael Knapp: Investigation, Methodology. Patrick Compton: Investigation. Loretta A. Fernandez: Resources, Supervision. Akram N. Alshawabkeh: Resources, Conceptualization, Supervision. Philip Larese-Casanova: Conceptualization, Supervision, Writing – review & editing, Project administration, Funding acquisition.

Declaration of Competing Interest

The authors declare that they have no known competing financial interests or personal relationships that could have appeared to influence the work reported in this paper.

Acknowledgements

This work was financially supported by the US Strategic Environmental Research and Development Program (project ER19-1130).

Additional support was provided by the Superfund Research Program of the National Institute of Environmental Health Sciences (NIEHS), National Institutes of Health (NIH; grant number P42ES017198). Special thanks to Michael MacNeil and Kurt Braun for reactor vessel fabrication. This work made use of the Cornell Center for Materials Research Shared Facilities which are supported through the NSF MRSEC Program (DMR-1719875). The authors thank Begüm Erdinçler for experimental assistance.

Appendix A. Supporting information

Supplementary data associated with this article can be found in the online version at doi:10.1016/j.jece.2022.107865.

References

- A.L. Juhasz, R. Naidu, Explosives: Fate, dynamics, and ecological impact in terrestrial and marine environments, Rev. Environ. Contam. Toxicol. 191 (2007) 163–215, https://doi.org/10.1007/978-0-387-69163-3 6.
- [2] C.M. Warner, K.A. Gust, J.K. Stanley, T. Habib, M.S. Wilbanks, N. Garcia-Reyero, E. J. Perkins, A systems toxicology approach to elucidate the mechanisms involved in RDX species-specific sensitivity, Environ. Sci. Technol. 46 (2012) 7790–7798, https://doi.org/10.1021/es300495c.
- [3] A.J. Kennedy, A.R. Poda, N.L. Melby, L.C. Moores, S.M. Jordan, K.A. Gust, A. J. Bednar, Aquatic toxicity of photo-degraded insensitive munition 101 (IMX-101) constituents, Environ. Toxicol. Chem. 36 (2017) 2050–2057, https://doi.org/10.1002/etc.3732.
- [4] G.R. Lotufo, J.K. Stanley, P. Chappell, N.L. Melby, M.S. Wilbanks, K.A. Gust, Subchronic, chronic, lethal and sublethal toxicity of insensitive munitions mixture formulations relative to individual constituents in Hyalella azteca, Chemosphere 210 (2018) 795–804, https://doi.org/10.1016/j.chemosphere.2018.07.049.
- [5] L.C. Moores, A.J. Kennedy, L. May, S.M. Jordan, A.J. Bednar, S.J. Jones, D. L. Henderson, L. Gurtowski, K.A. Gust, Identifying degradation products responsible for increased toxicity of UV-Degraded insensitive munitions, Chemosphere 240 (2020), https://doi.org/10.1016/j.chemosphere.2019.124958.
- [6] J.D. Arthur, N.W. Mark, S. Taylor, J. Šimůnek, M.L. Brusseau, K.M. Dontsova, Dissolution and transport of insensitive munitions formulations IMX-101 and IMX-104 in saturated soil columns, Sci. Total Environ. 624 (2018) 758–768, https://doi. org/10.1016/j.scitotenv.2017.11.307.
- [7] W. Fawcett-Hirst, T.J. Temple, M.K. Ladyman, F. Coulon, Adsorption behaviour of 1,3,5-trinitroperhydro-1,3,5-triazine, 2,4-dinitroanisole and 3-nitro-1,2,4-triazol-5one on commercial activated carbons, Chemosphere 255 (2020), 126848, https:// doi.org/10.1016/j.chemosphere.2020.126848.
- [8] P. Wanaratna, C. Christodoulatos, M. Sidhoum, Kinetics of RDX degradation by zero-valent iron (ZVI), J. Hazard. Mater. 136 (2006) 68–74, https://doi.org/ 10.1016/J.JHAZMAT.2005.11.015.
- [9] A. Koutsospyros, J. Pavlov, J. Fawcett, D. Strickland, B. Smolinski, W. Braida, Degradation of high energetic and insensitive munitions compounds by Fe/Cu bimetal reduction, J. Hazard. Mater. 219–220 (2012) 75–81, https://doi.org/ 10.1016/j.jhazmat.2012.03.048.
- [10] J. Shen, C. Ou, Z. Zhou, J. Chen, K. Fang, X. Sun, J. Li, L. Zhou, L. Wang, Pretreatment of 2,4-dinitroanisole (DNAN) producing wastewater using a combined zero-valent iron (ZVI) reduction and Fenton oxidation process, J. Hazard. Mater. 260 (2013) 993–1000, https://doi.org/10.1016/j. ibayrant 2013 07 003
- [11] V.K. Balakrishnan, A. Halasz, J. Hawari, Alkaline hydrolysis of the cyclic nitramine explosives RDX, HMX, and CL-20: New insights into degradation pathways obtained by the observation of novel intermediates, Environ. Sci. Technol. 37 (2003) 1838–1843, https://doi.org/10.1021/es020959h.
- [12] A.J. Salter-Blanc, E.J. Bylaska, J.J. Ritchie, P.G. Tratnyek, Mechanisms and kinetics of alkaline hydrolysis of the energetic nitroaromatic compounds 2,4,6-trinitrotoluene (TNT) and 2,4-dinitroanisole (DNAN), Environ. Sci. Technol. 47 (2013) 6790–6798, https://doi.org/10.1021/es304461t.
- [13] L. Sviatenko, C. Kinney, L. Gorb, F.C. Hill, A.J. Bednar, S. Okovytyy, J. Leszczynski, Comprehensive investigations of kinetics of alkaline hydrolysis of TNT (2,4,6trinitrotoluene), DNT (2,4-dinitrotoluene), and DNAN (2,4-dinitroanisole), Environ. Sci. Technol. 48 (2014) 10465–10474, https://doi.org/10.1021/ es5026678.
- [14] P. Bose, W.H. Glaze, D.S. Maddox, Degradation of RDX by various advanced oxidation processes: I. Reaction rates, Water Res 32 (1998) 997–1004, https://doi. org/10.1016/S0043-1354(97)00307-2.
- [15] D.N. Khue, T.D. Lam, N. Van Chat, V.Q. Bach, D.B. Minh, V.D. Loi, N. Van Anh, Simultaneous degradation of 2,4,6-trinitrophenyl-N-methylnitramine (Tetryl) and hexahydro-1,3,5-trinitro-1,3,5 triazine (RDX) in polluted wastewater using some advanced oxidation processes, J. Ind. Eng. Chem. 20 (2014) 1468–1475, https:// doi.org/10.1016/j.jiec.2013.07.033.
- [16] H. Su, C. Christodoulatos, B. Smolinski, P. Arienti, G. O'Connor, X. Meng, Advanced oxidation process for DNAN using UV/H₂O₂, Engineering 5 (2019) 849–854, https://doi.org/10.1016/j.eng.2019.08.003.

- [17] P.M.L. Bonin, D. Bejan, L. Schutt, J. Hawari, N.J. Bunce, Electrochemical reduction of Hexahydro-1,3,5-trinitro-1,3,5-triazine in aqueous solutions, Environ. Sci. Technol. 38 (2004) 1595–1599, https://doi.org/10.1021/es0305611.
- [18] R.B. Doppalapudi, G.A. Sorial, S.W. Maloney, Electrochemical reduction of 2,4-dinitrotoluene in a continuous flow laboratory scale reactor, J. Environ. Eng. 129 (2003) 192–201, https://doi.org/10.1061/(ASCE)0733-9372(2003)129:3(192).
- [19] A.H. Wani, B.R. O'Neal, D.M. Gilbert, D.B. Gent, J.L. Davis, Electrolytic transformation of ordinance related compounds (ORCs) in groundwater: laboratory mass balance studies, Chemosphere 62 (2006) 689–698, https://doi.org/10.1016/ j.chemosphere.2005.06.012.
- [20] D.B. Gent, A.H. Wani, J.L. Davis, A. Alshawabkeh, Electrolytic redox and electrochemical generated alkaline hydrolysis of hexahydro-1,3,5-trinitro-1,3,5 triazine (RDX) in sand columns, Environ. Sci. Technol. 43 (2009) 6301–6307, https://doi.org/10.1021/es803567s.
- [21] D.B. Gent, A. Wani, A.N. Alshawabkeh, Experimental design for one dimensional electrolytic reactive barrier for remediation of munition constituent in groundwater, Electrochim. Acta (2012) 130–137, https://doi.org/10.1016/j. electacta.2012.04.043.
- [22] Y. Chen, L. Hong, W. Han, L. Wang, X. Sun, J. Li, Treatment of high explosive production wastewater containing RDX by combined electrocatalytic reaction and anoxic-oxic biodegradation, Chem. Eng. J. 168 (2011) 1256–1262, https://doi. org/10.1016/j.cej.2011.02.032.
- [24] D.K. Palaniswamy, G.A. Sorial, S.W. Maloney, Electrochemical reduction of 2,4,6-Trinitrotoluene, Environ. Eng. Sci. 21 (2004) 203–218, https://doi.org/10.1089/ 109287504773087372
- [25] J.D. Rodgers, N.J. Bunce, Electrochemical treatment of 2,4,6-trinitrotoluene and related compounds, Environ. Sci. Technol. 35 (2001) 406–410, https://doi.org/ 10.1021/es001465s.
- [26] M.P. Cronin, A.I. Day, L. Wallace, Electrochemical remediation produces a new high-nitrogen compound from NTO wastewaters, J. Hazard. Mater. 149 (2007) 527–531, https://doi.org/10.1016/j.jhazmat.2007.08.007.
- [27] Y. Chen, L. Hong, W. Han, L. Wang, X. Sun, J. Li, Treatment of high explosive production wastewater containing RDX by combined electrocatalytic reaction and anoxic-oxic biodegradation, Chem. Eng. J. 168 (2011) 1256–1262, https://doi. org/10.1016/j.cei.2011.02.032.
- [28] L. Wallace, M.P. Cronin, A.I. Day, D.P. Buck, Electrochemical method applicable to treatment of wastewater from nitrotriazolone production, Environ. Sci. Technol. 43 (2009) 1993–1998. https://doi.org/10.1021/es8028878.
- [29] C.L. Madeira, W.M. Kadoya, G. Li, S. Wong, R. Sierra-Alvarez, J.A. Field, Reductive biotransformation as a pretreatment to enhance in situ chemical oxidation of nitroaromatic and nitroheterocyclic explosives, Chemosphere 222 (2019) 1025–1032, https://doi.org/10.1016/j.chemosphere.2019.01.178.
- [30] K. Ayoub, S. Nélieu, E.D. Van Hullebusch, J. Labanowski, I. Schmitz-Afonso, A. Bermond, M. Cassir, Electro-Fenton removal of TNT: Evidences of the electro-chemical reduction contribution, Appl. Catal. B Environ. 104 (2011) 169–176, https://doi.org/10.1016/j.apcatb.2011.02.016.
- [31] R. Khatiwada, C. Olivares, L. Abrell, R.A. Root, R. Sierra-Alvarez, J.A. Field, J. Chorover, Oxidation of reduced daughter products from 2,4-dinitroanisole (DNAN) by Mn(IV) and Fe(III) oxides, Chemosphere 201 (2018) 790–798, https://doi.org/10.1016/j.chemosphere.2018.03.020.
- [32] J.M. Thomas, R. Hernandez, C.H. Kuo, Single-step treatment of 2,4-dinitrotoluene via zero-valent metal reduction and chemical oxidation, J. Hazard. Mater. 155 (2008) 193–198, https://doi.org/10.1016/j.jhazmat.2007.11.073.
- [33] L. Rajic, N. Fallahpour, E. Oguzie, A. Alshawabkeh, Electrochemical transformation of thichloroethylene in groundwater by Ni-containing cathodes, Electrochim. Acta 181 (2015) 118–122, https://doi.org/10.1016/j. electracta.2015.03.112.
- [34] J. He, A.E. Sáez, W.P. Ela, E.A. Betterton, R.G. Arnold, Destruction of aqueousphase carbon tetrachloride in an electrochemical reactor with a porous cathode, Ind. Eng. Chem. Res. 43 (2004) 913–923, https://doi.org/10.1021/ie030591c.
- [35] M.E. Fuller, C.E. Schaefer, J.M. Lowey, Degradation of explosives-related compounds using nickel catalysts, Chemosphere 67 (2007) 419–427, https://doi. org/10.1016/j.chemosphere.2006.10.002.
- [36] Y. Zhang, M.D. Merrill, B.E. Logan, The use and optimization of stainless steel mesh cathodes in microbial electrolysis cells, Int. J. Hydrog. Energy 35 (2010) 12020–12028, https://doi.org/10.1016/J.IJHYDENE.2010.08.064.
- [37] G.C. Hale, The nitration of hexamethylaminetetramine, J. Am. Chem. Soc. 47 (1925) 2754–2763, https://doi.org/10.1021/JA01688A017.
- [38] W. Zhou, L. Rajic, L. Chen, K. Kou, Y. Ding, X. Meng, Y. Wang, B. Mulaw, J. Gao, Y. Qin, A.N. Alshawabkeh, Activated carbon as effective cathode material in iron-free Electro-Fenton process: integrated H₂O₂ electrogeneration, activation, and pollutants adsorption, Electrochim. Acta 296 (2019) 317–326, https://doi.org/10.1016/J.ELECTACTA.2018.11.052.
- [39] D.M. Gilbert, T.C. Sale, Sequential electrolytic oxidation and reduction of aqueous phase energetic compounds, Environ. Sci. Technol. 39 (2005) 9270–9277, https:// doi.org/10.1021/es051452k.
- [40] J. Hawari, F. Monteil-Rivera, N.N. Perrault, A. Halasz, L. Paquet, Z. Radovic-Hrapovic, S. Deschamps, S. Thiboutot, G. Ampleman, Environmental fate of 2,4dinitroanisole (DNAN) and its reduced products, Chemosphere 119 (2015) 16–23, https://doi.org/10.1016/J.chemosphere.2014.05.047.
- [41] C.I. Olivares, J. Wang, C.D. Silva Luna, J.A. Field, L. Abrell, R. Sierra-Alvarez, Continuous treatment of the insensitive munitions compound N-methyl-p-nitro aniline (MNA) in an upflow anaerobic sludge blanket (UASB) bioreactor,

- Chemosphere 144 (2016) 1116–1122, https://doi.org/10.1016/j.chemosphere.2015.09.092.
- [42] J.B. Niedźwiecka, S.R. Drew, M.A. Schlautman, K.A. Millerick, E. Grubbs, N. Tharayil, K.T. Finneran, Iron and electron shuttle mediated (bio)degradation of 2,4-dinitroanisole (DNAN), Environ. Sci. Technol. 51 (2017) 10729–10735, https://doi.org/10.1021/ACS.EST.7B02433.
- [43] J. Sun, Y. Fu, G. He, X. Sun, X. Wang, Catalytic hydrogenation of nitrophenols and nitrotoluenes over a palladium/graphene nanocomposite, Catal. Sci. Technol. 4 (2014) 1742–1748, https://doi.org/10.1039/C4CY00048J.
- [44] E.A. Gelder, S.D. Jackson, C.M. Lok, The hydrogenation of nitrobenzene to aniline: a new mechanism, Chem. Commun. (2005) 522–524, https://doi.org/10.1039/ R411603H
- [45] S.Y. Oh, D.K. Cha, P.C. Chiu, Graphite-mediated reduction of 2,4-dinitrotoluene with elemental iron, Environ. Sci. Technol. 36 (2002) 2178–2184, https://doi.org/ 10.1021/FS011474G.
- [46] H.M. Heilmann, U. Wiesmann, M.K. Stenstrom, Kinetics of the alkaline Hydrolysis of high explosives RDX and HMX in aqueous solution and adsorbed to activated carbon, Environ. Sci. Technol. 30 (1996) 1485–1492, https://doi.org/10.1021/ FS95.04101
- [47] C. Wang, A.F. Wallace, L. Heraty, H. Qi, N.C. Sturchio, Alkaline hydrolysis pathway of 2,4-dinitroanisole verified by ¹⁸O tracer experiment, J. Hazard. Mater. 396 (2020), 122627, https://doi.org/10.1016/J.JHAZMAT.2020.122627.
- [48] D. Fournier, A. Halasz, J. Spain, R.J. Spanggord, J.C. Bottaro, J. Hawari, Biodegradation of the hexahydro-1,3,5-Trinitro-1,3,5-triazine ring cleavage product 4-nitro-2,4-diazabutanal by Phanerochaete chrysosporium, Appl. Environ. Microbiol. 70 (2004) 1123–1128, https://doi.org/10.1128/AEM.70.2.1123-1128.2004.
- [49] C. Chokejaroenrat, S.D. Comfort, C.E. Harris, D.D. Snow, D. Cassada, C. Sakulthaew, T. Satapanajaru, Transformation of hexahydro-1,3,5-trinitro-1,3,5-

- triazine (RDX) by permanganate, Environ. Sci. Technol. 45 (2011) 3643–3649, https://doi.org/10.1021/ES104057V/SUPPL_FILE/ES104057V_SL_001.PDF.
- [50] P. Larese-Casanova, M.M. Scherer, Abiotic transformation of hexahydro-1,3,5-trinitro-1,3,5-triazine (RDX) by green rusts, Environ. Sci. Technol. 42 (2008) 3975–3981, https://doi.org/10.1021/es702390b.
- [51] L.S. Hundal, J. Singh, E.L. Bier, P.J. Shea, S.D. Comfort, W.L. Powers, Removal of TNT and RDX from water and soil using iron metal, Environ. Pollut. 97 (1997) 55–64, https://doi.org/10.1016/S0269-7491(97)00081-X.
- [52] P. Bose, W.H. Glaze, D.S. Maddox, Degradation of RDX by various advanced oxidation processes: I. Reaction rates, Water Res 32 (1998) 997–1004, https://doi. org/10.1016/S0043-1354(97)00307-2.
- [53] Y. Liu, S. Chen, X. Quan, H. Yu, Efficient Electrochemical reduction of carbon dioxide to acetate on nitrogen-doped nanodiamond, J. Am. Chem. Soc. 137 (2015) 11631–11636, https://doi.org/10.1021/JACS.5B02975.
- [54] N.N. Perreault, A. Halasz, D. Manno, S. Thiboutot, G. Ampleman, J. Hawari, Aerobic mineralization of nitroguanidine by Variovorax strain VC1 isolated from soil, Environ. Sci. Technol. 46 (2012) 6035–6040, https://doi.org/10.1021/ es301047d.
- [55] C.I. Olivares, L. Abrell, R. Khatiwada, J. Chorover, R. Sierra-Alvarez, J.A. Field, Bio)transformation of 2,4-dinitroanisole (DNAN) in Soils, J. Hazard. Mater. 304 (2016) 214, https://doi.org/10.1016/J.JHAZMAT.2015.10.059.
- [56] A. Barroux, T. Duguet, N. Ducommun, E. Nivet, J. Delgado, L. Laffont, C. Blanc, Combined XPS / TEM study of the chemical composition and structure of the passive film formed on additive manufactured 17-4PH stainless steel, Surf. Interfaces 22 (2021), 100874, https://doi.org/10.1016/J.SURFIN.2020.100874.
- [57] F. Jiménez-Villacorta, Y. Huttel, A. Muñoz-Martín, C. Ballesteros, E. Román, C. Prieto, Core-shell nanocrystalline structures in oxidized iron thin films prepared by sputtering at very low temperatures, J. Appl. Phys. 101 (2007), https://doi.org/ 10.1063/1.2737389.